Taylor & Francis
Taylor & Francis Group

International Journal of Ambient Energy

Innovation in Temperature-Dependent Inclined MHD Radiative Micropolar Casson Hybrid Nanofluid Flow over a Stretching Sheet/Cylinder

Submission ID	257612684
Article Type	Research Article
Keywords	Casson Micropolar Hybrid nanofluid, Inclined magnetic field, Variable Thermal conductivity and Viscosity, Radiation and Heat generation, Numerical approach.
Authors	Nadeem Abbas, Wasfi Shatanawi, Taqi A. M. Shatnawi

Innovation in Temperature-Dependent Inclined MHD Radiative Micropolar Casson Hybrid Nanofluid Flow over a Stretching Sheet/Cylinder

Nadeem Abbas[a], Wasfi Shatanawi[a,b], Taqi A.M. Shatnawi[b]*
[a]Department of Mathematics and Sciences, College of Humanities and Sciences, Prince Sultan University, Riyadh, 11586, Saudi Arabia
[b]Department of Mathematics, Faculty of Science, The Hashemite University, P.O Box 330127, Zarqa 13133, Jordan
[*]Corresponding author nabbas@psu.edu.sa

Abstract

We investigated the flow and heat transfer characteristics of Casson-Micropolar hybrid nanofluid over a stretching sheet/cylinder, incorporating Joule heating, thermal radiation, and variations in thermal conductivity and viscosity. The nanoparticles of Ag and CuO with base fluid EG(Ethylene Glycol) are discussed. Additionally, the study explores the impact of an inclined magnetic field on the flow behavior. The governing partial differential equations describe the conservation of mass, energy, and momentum which are transformed into a nonlinear ordinary differential equation by means of appropriate similarity transformations. These equations are then cracked numerically using a reliable computational technique. The study reveals significant influences of hybrid nanofluid properties on the velocity, temperature, and microrotation profiles. The inclined magnetic field significantly affects fluid dynamics, leading to flow resistance and thermal performance variations. The results highlight the importance of these factors in enhancing the thermal efficiency of systems using hybrid nanofluid. The heat transfer of sheet achieved more as compared to stretching cylinder.

Keywords: Casson Micropolar Hybrid nanofluid; Inclined magnetic field; Variable Thermal conductivity and Viscosity; Radiation and Heat generation; Numerical approach.

1 Introduction

Micropolar fluid theory enhances classical fluid mechanics by accounting for microstructural effects in fluids containing microscale suspended particles. These fluids exhibit micro-rotation and rotational inertia, making the theory highly applicable to complex fluids such as blood, polymeric solutions, and liquid crystals. A notable application of micropolar fluid mechanics lies in biomedical engineering, particularly in the development of advanced prosthetic devices and synthetic organs. For example, micropolar fluid theory provides more accurate representations of blood behavior in modeling blood flow through microvascular networks, accounting for the rotational motion of red blood cells, which classical fluid models cannot capture. This improved understanding aids in developing more effective medical devices that better mimic natural blood flow, enhancing patient outcomes in various medical treatments. The initial idea about the micropolar fluid theory was presented by Erimgen [1]. He made

noteworthy improvements in fluid mechanics by reviewing the behavior of micropolar fluids in the occurrence of stretching surfaces. Kazakia and Ariman [2] have extended the characteristics of micropolar fluid behavior and expanded the understanding of these complex fluids beyond their mechanical characteristics. They are characterized by their microstructure and the presence of intrinsic angular momentum. Char and Chang [3] reported the features of micropolar fluid in the presence of natural convection. They also discussed the micropolar fluid using the flat plate within wall conduction. Tomar and Kumar [4] discussed the impact of elastic wave propagation using the cylindrical bore under the micropolar fluid. They developed analytical solutions and discussed the implications of their findings for material science and engineering applications, where micropolar elasticity plays a crucial role. Elbarbary and Elgazery [5] developed the numerical results for stagnation flow using the micropolar fluid. The variable properties have been studied in their analysis at stretchable cylinder. Rehman et al. [6] studied a micropolar fluid's flow and heat transfer at a stretchable cylinder having vertical exponentially. They focused on how stretching affects fluid flow and heat transfer features, highlighting the interaction between microstructural properties and boundary layer dynamics. Abbas et al. [7] investigated the flow of a micropolar nanofluid around a circular cylinder having stagnation point and slip phenomena. The research explored how nanoparticle additives influence flow and heat transfer, with implications for thermal management and nanofluid applications. Khan et al. [8] examined non-Newtonian-based micropolar fluid flow over a nonlinear stretching cylinder having Soret and Dufour number impacts. Their work extended the understanding of micropolar fluid behavior in nonlinear flow regimes, highlighting the impact of thermal and mass diffusion on flow characteristics. Recently, few authors have been developed the models using the micropolar for different assumptions see Refs. [9-10].

Nanofluid is created by adding very small particles to base fluids such as ethylene glycol, water or oil. Nanofluids have improved thermal characteristics, with higher heat transfer coefficients and thermal conductivity. This improvement is due to the nanoparticles' high surface area to volume ratio, which allows for better interaction with the base fluid. One practical use of nanofluids is in cooling high-power electronics and microprocessors, where efficient heat dissipation is crucial. For example, by incorporating nanofluids into the cooling systems of data centres, the improved thermal conductivity allows more effective removal of heat generated by densely packed electronic components. This enhances the reliability and performance of electronic devices and supports energy efficiency by reducing the need for additional cooling infrastructure. Ultimately, this contributes to sustainable and

high-performance computing solutions. Due to several real-life applications, Choi and Eastman [11] considered the mixture of simple fluid with solid nanosized particles. This analysis developed several ideas because a lot of attention was achieved. The base fluid and nanoparticle mixture gained a higher heat transfer rate than ordinary fluid. Li and Kleinstreuer [12] worked on the Choi and Eastman [11] model. They discussed the thermal performance using the microchannel. Gorla et al. [12] highlighted the impact of nanofluid using stretchable surfaces in the cylindrical form. Several authors did study the development in heat transfer enhancement about more performance higher achieve heat. During this analysis, the word hybrid nanofluid developed. Hybrid nanofluid, which combines two or more different kinds of nanoparticles suspended in a base fluid, offers improved thermal properties compared to traditional nanofluid. The combined effect of the various properties of the mixed nanoparticles improves thermal conductivity, heat transfer abilities, and stability. The applications of hybrid nanofluid include use in electronic devices and advanced cooling systems for high-volume automotive engines. Al2O3–Cu/water hybrids synthesized through advanced methods was calculated by Suresh et al. [13]. Sarkar et al. [14] have comprehensively reviewed various applications of hybrid nanofluids in renewable energy and thermal systems. Huminic and Huminic 15] investigated hybrid nanofluid flow with entropy generation. Furthermore, recent studies have expanded the exploration of hybrid nanofluids to magnetic fields and biomedical applications. Alghamdi et al. [16] deliberated the influence of hybrid nanomaterial flow of MHD at stretchable surface. Alsaedi et al. [17] investigated the influence of magnetic fields with hybrid nanofluid flow. Some authors have recently developed models using hybrid nanofluid under different assumptions (see Refs. [18-19]).

Casson fluid model defines the behavior of non-Newtonian fluid with yield stress. Below stress, the fluid acts like a solid, and above it, it flows like a viscous fluid. This model is particularly helpful in predicting the flow of substances like blood, chocolate, and certain cosmetic products. One of the practical applications of Casson fluid mechanics is in hemodynamic, where it is used to study blood flow in arteries. Casson model is more effective for dual behavior since blood has both solid and fluid properties due to the presence of plasma and red blood cells. Casson fluid mechanics is applied in biomedical engineering and is crucial for accurate blood flow simulations. The researchers led to improved designs for medical devices, such as stents and artificial heart valves. Batra and Das [20] initiated the stress tensor for Casson fluid model and implemented on the rotating cylinder. Pandey and Tripathi [21] outlined the features of a Casson fluid in the peristaltic model using a finite channel. Malik et al. [22] deliberated the Casson nanofluid at an exponentially vertical stretchable cylinder.

Tulu and Ibrahim [23] used the spectral relaxation technique to analyze Casson nanofluid. Their investigation emphasized the importance of considering non-Fourier heat conduction effects to predict heat transfer rates in Casson nanofluid systems accurately. Dawar et al. [24] reported the inspiration of gyrotactic microorganisms and magnetic fields on Casson fluid flow over a stratified stretching cylinder. Nawaz et al. [25] conducted a predictor-corrector technique to analyze the electrical MHD flow of Casson nanofluids. Arif et al. [26] designed a finite difference method coupled with a neural network approach to study Casson nanofluid flow. Some authors have recently developed models using Casson fluid under different assumptions (see Refs. [27-28]).

The analysis of fluid flow over a stretching cylinder is a significant area of study in fluid dynamics because it has practical applications in industrial processes. The stretching process develops heat and mass transfer rates, making it important in wire drawing, polymer extrusion, and glass fiber production. An actual application is manufacturing optical fibers, where precise control of the surface quality and cooling rate is crucial. Engineers must understand the fluid flow and heat transfer characteristics over a stretching cylinder. The influential work by Wang [29] delved into the fluid flow produced by a stretchable cylinder. Ishak et al. [30] examined the impacts of uniform suction and blowing on flow with heat transfer at a stretching cylinder. Mastroberardino and Paullet [31] investigated the steady stagnation flow at stretching cylinder. Malik et al. [32] studied the flow and heat transfer features of magnetohydrodynamic (MHD) Sisko fluid at a stretching cylinder. Usman et al. [33] examined the effects of velocity and thermal slip on Casson nanofluid flow over an inclined permeable stretching cylinder. Bilal et al. [34] performed of fluid flow at a stretching cylinder. Recently, authors have developed the results about stretching cylinder under flow assumptions (see Refs. [35-37]).

This study aims to uncover the potential of hybrid nanofluid in Casson micropolar fluid over a stretching sheet/cylinder offers transformative potential for advanced thermal management. Hybrid nanofluids enhance thermal conductivity, while Joule heating and thermal radiation affect heat transfer. Variable thermal conductivity and viscosity add complexity, making optimization crucial. An inclined magnetic field provides an additional control mechanism, influencing flow and heat transfer. The governing differential equations are defining the conservation of momentum, mass, and energy which are altered into a nonlinear ordinary differential equation using appropriate similarity transformations. These equations are then cracked numerically using a reliable computational technique. The study reveals significant influences of hybrid nanofluid properties on the velocity,

temperature, and microrotation profiles. The findings will lead to innovative engineering designs and optimization strategies, driving technological advancements in thermal engineering.

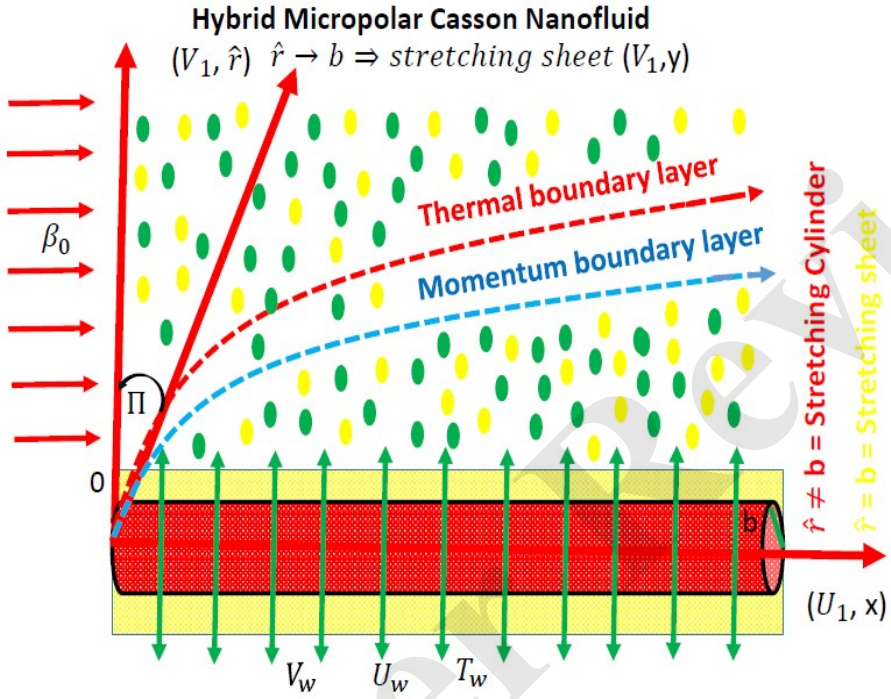

Fig. 1: Flow pattern over stretching sheet/cylinder.

2 Mathematical formulation

Steady flow of incompressible hybrid micropolar casson nanofluid flow over a permeable stretching cylinder/sheet is considered which is seen in Fig. 1. Thermal radiation and temperature dependents properties have been considered in the present analysis. The accurate angle of inclined magnetic field Π applying with y-direction. As the $\Pi = \frac{\pi}{2}$, the magnetic field behaves as a transverse magnetic field. U_1 and V_1 are the velocity components along the axial and radial direction in case of stretching cylinder (in case of stretching sheet in $x-$, $y-$ directions). The flow is expected to be in the axial (x) direction, with the radial direction being normal to x. The entire analysis is conducted under the expectations of boundary layer theory. The expression is presented as (see Refs. [38-39]):

$$\frac{\partial V_1}{\partial \hat{r}} + \frac{V_1}{\hat{r}} + \frac{\partial U_1}{\partial x} = 0, \tag{1}$$

$$\rho_{hNF}\left(U_1\frac{\partial U_1}{\partial x}+V_1\frac{\partial U_1}{\partial \hat{r}}\right)$$
$$=\frac{1}{\hat{r}}\frac{\partial}{\partial \hat{r}}\left(\hat{r}\left(\mu_{hNF}(T)+\frac{P_{\hat{r}}}{\sqrt{2\pi_c}}+k^*\right)\frac{\partial U_1}{\partial \hat{r}}\right)-\sigma_{hNF}{\beta_0}^2U_1\sin^2(\Pi)+k^*\frac{\partial(N\hat{r})}{\partial \hat{r}}-\frac{\nu_h}{k} \quad (2)$$
$$\frac{\partial U_1}{\partial \hat{r}},$$
$$\rho_{hNF}j\left(U_1\frac{\partial N}{\partial x}+V_1\frac{\partial N}{\partial \hat{r}}\right)=\gamma_{hNF}\frac{1}{\hat{r}}\frac{\partial}{\partial \hat{r}}\left(\hat{r}\frac{\partial N}{\partial \hat{r}}\right)-k^*\left(2N+\frac{\partial U_1}{\partial \hat{r}}\right), \quad (3)$$
$$U_1\frac{\partial T}{\partial x}+\ V_1\frac{\partial T}{\partial \hat{r}}=\frac{1}{(\rho c_p)_{hnf}}\frac{1}{\hat{r}}\frac{\partial}{\partial \hat{r}}\left(K_{hNF}(T)\hat{r}\frac{\partial T}{\partial \hat{r}}\right)+\frac{1}{(\rho c_p)_{hNF}}R_1(T-\ T_\infty)-\frac{1}{(\rho c_p)_{hNF}}\frac{1}{\hat{r}}\frac{\partial(\hat{r}}{\partial} \quad (4)$$

With the following suitable boundary conditions:

$$U_1=U_w,\quad N_1=-n\frac{\partial U_1}{\partial \hat{r}},\ V_1=V_w,\ T-T_w=0,\ at\ \ \hat{r}\to b,$$
$$U_1\to 0,\ T\to T_\infty,\ N_1\to 0,\ as\ \hat{r}\to\infty. \quad (5)$$

Where, $\gamma_1=\mu_B\frac{\sqrt{2\pi_c}}{P_{\hat{r}}}$ is Casson fluid parameter. $\gamma_{hNF}=\mu_{hNF}(T)+\frac{k^*}{2}$ is the viscosity of spin radiation of hybrid nanofluid. $\mu_{hNF}(T)=\mu_{hNF}(1-M\Theta(\xi))$ is variable viscosity of hybrid nanofluid. $K_{HNF}(T)=k_{hNF}(1+E\Theta(\xi))$ is the variable thermal conductivity of hybrid nanofluid. σ_{hNF} is electric conductivity of hybrid nanofluid. The thermal expansion coefficient is β_0. $q_{\hat{r}}$ is heat flux of radiative. The Reynold approximation of heat flux of radiative is presented as $q_{\hat{r}}=-\frac{4\sigma^*\partial T^4}{3k_1\,\partial \hat{r}}$. The constant Steffen Boltzmann is σ^*. k_1 is absorption coefficient. Differences of Temperature within the flow are considered to be sufficiently small, so T^4 presented as a temperature linear function. The T^4 expanding using the Taylor series about T_∞ and diminished the higher order terms consider as ${T^4}\cong 4{T_\infty}^3T-3\ {T_\infty}^4$. The special transformation have been introduced as following:

$$U_1=\ \frac{U_0x}{l}H_\xi(\xi),\ V_1=\ -\frac{b}{\upsilon_f}\sqrt{\frac{\upsilon_fU_0}{l}},\ \xi=\frac{\hat{r}^2-b^2}{2b}\sqrt{\frac{U_0}{\upsilon_f l}},\ N=\sqrt[3]{\frac{U_0}{l}}\frac{x\hat{r}}{b\sqrt{\upsilon_f}}G(\xi),\qquad T=\ T$$
$$+\ (T_w-\ T_\infty)\Theta(\xi). \quad (6)$$

The non-dimensional equations are become as

$$\frac{\rho_F}{\rho_{hNF}}\frac{\mu_{hNF}}{\mu_F}\left(1+\frac{1}{\gamma_1}+\chi\right)\Big((1+2\xi\mathrm{A})(1-M\Theta(\xi))H_{\xi\xi\xi}(\xi)+2A(1-M\Theta(\xi))H_{\xi\xi}(\xi)-M(1+$$
$$H_{\xi\xi}(\xi)\Theta_\xi(\xi)\Big)+H_{\xi\xi}(\xi)H(\xi)-\left(H_\xi(\xi)\right)^2-\lambda\frac{\rho_F}{\rho_{hNF}}\frac{\mu_{hNF}}{\mu_F}(1-M\Theta(\xi))H_\xi(\xi)-\lambda \quad (7)$$
$$H_\xi(\xi)\sin^2(\Pi)+\chi\frac{\rho_F}{\rho_{hNF}}\big((1+2\xi\mathrm{A})G_\xi(\xi)+2AG(\xi)\big)=0,$$

$$\frac{\rho_F}{\rho_{hNF}}\left(\frac{\mu_{hNF}}{\mu_F}+\frac{\chi}{2}\right)\big((1+2\xi\mathrm{A})(1-M\Theta(\xi))G_{\xi\xi}(\xi)+4A(1-M\Theta(\xi))G_{\xi}(\xi)-M(1+2\xi\mathrm{A})G_{\xi}(\xi)\big)+G_{\xi}(\xi)H(\xi)-AG(\xi)H(\xi)-2H_{\xi}(\xi)G(\xi)-\frac{\chi}{2}\frac{\rho_F}{\rho_{hNF}}\big(G(\xi)+H_{\xi\xi}(\xi)\big)=0, \quad (8)$$

$$\frac{1}{Pr}\frac{(\rho c_p)_F}{(\rho c_p)_{hNF}}\frac{k_{hNF}}{k_F}\big((1+2\xi\mathrm{A})(1+E\Theta(\xi))\Theta_{\xi\xi}(\xi)+2A(1+E\Theta(\xi))\Theta_{\xi}(\xi)+E(1+2\xi\mathrm{A})\Theta_{\xi}(\xi)\big)+\frac{4}{3}Rd\big((1+2\xi\mathrm{A})\Theta_{\xi\xi}(\xi)+2A\Theta_{\xi}(\xi)\big)+\Theta_{\xi}(\xi)H(\xi)-2H_{\xi}(\xi)\Theta(\xi)+S\frac{(\rho c_{\mathrm{l}}}{(\rho c_p)}\xi)=0, \quad (9)$$

With boundary condition

$$H(0)=Q,\ H_{\xi}(0)=1,\ H_{\xi}(\infty)=1,\Theta(0)-1=0,\quad G(0)=-nH_{\xi\xi}(0),\quad G(\infty)=0,\qquad \Theta(\propto \quad (10)$$

Table 1: Thermodynamic properties of fluid and particles (see Ref. [39]).

	c_p(Heat Capacity)	ρ(Density)	k(Thermal Conductivity)	Pr(Prandtl Number)	σ(Electric Conductivity)
$Ethylene\ glycol$	2382.1	1117.48	0.2492	210.3	1.07×10^{-8}
Ag	233	10500	429		6.3×10^{-7}
CuO	531.8	6320	76.5		5.8×10^{-7}

The thermodynamic properties are detailed in Table 1, with the thermodynamic expressions for nanoparticles and the base fluid provided as follows:

$$\rho_{hNF}=(1-\phi_{Ag})(1-\phi_{CuO})\rho_{EG}+\phi_{Ag}\rho_{Ag}+\phi_{CuO}\rho_{CuO},$$

$$(c_p\rho)_{hNF}=(1-\phi_{Ag})(1-\phi_{CuO})(c_p\rho)_{EG}+\phi_{Ag}(c_p\rho)_{Ag}+\phi_{CuO}(c_p\rho)_{CuO},$$

$$k_{hNF}=\frac{k_{Ag}+2k_{BF}-2\phi_{Ag}(k_{BF}-k_{Ag})}{k_{Ag}+2k_{BF}+\phi_{Ag}(k_{BF}-k_{Ag})}k_{BF},$$

$$k_{BF}=\frac{k_{CuO}+2k_{EG}-2\phi_{CuO}(k_{EG}-k_{CuO})}{k_{CuO}+2k_{EG}+\phi_{CuO}(k_{EG}-k_{CuO})}k_{EG},$$

$$\sigma_{hNF}=\frac{\sigma_{Ag}+2\sigma_{BF}-2\phi_{Ag}(\sigma_{BF}-\sigma_{Ag})}{\sigma_{Ag}+2\sigma_{BF}+\phi_{Ag}(\sigma_{BF}-\sigma_{Ag})}\sigma_{BF},$$

$$\sigma_{BF}=\frac{\sigma_{CuO}+2\sigma_{EG}-2\phi_{CuO}(\sigma_{EG}-\sigma_{CuO})}{\sigma_{CuO}+2\sigma_{EG}+\phi_{CuO}(\sigma_{EG}-\sigma_{CuO})}\sigma_{EG}.$$

Nomenclature

Density of hybrid nanofluid	ρ_{hNF}	Heat capacity of CuO	$(c_p)_{CuO}$
Solid nanoparticle of Ag	ϕ_{Ag}	Heat Capacity of Ag	$(c_p)_{Ag}$
Solid nanoparticle of CuO	ϕ_{CuO}	Heat Capacity of Ethylene glycol	$(c_p)_{EG}$
Density of Ethylene glycol	ρ_{EG}	Thermal conductivity of Ag	k_{Ag}
Density of CuO	ρ_{CuO}	Thermal conductivity of CuO	k_{CuO}
Electric conductivity of CuO	σ_{CuO}	Thermal conductivity of Ethylene glycol	k_{EG}
Electric conductivity of Ag	σ_{BF}	Electric conductivity of Ethylene glycol	σ_{BF}

Casson fluid parameter	γ_1	Viscosity of spin hybrid nanofluid	γ_{hNF}
Thermal expansion coefficient	β_0	Constant of Steffen Boltzmann	σ^*
Wall temperature	T_w	Absorption coefficient	k_1
Temperature	T	Wall velocity	U_w
Velocity components	U_1, V_1	Micropolar component	N
Fluid constant	n	Vortex viscosity	k^*
Variable viscosity	M	Curvature factor	A
Porosity factor	λ	Variable thermal conductivity	E
Micropolar factor	χ	Magnetic field	Δ
Radiation	Rd	Casson fluid factor	γ_1
Temperature profile	Θ	Heat generation	S
Micro-rotation profile	G	Velocity profile	H

The physical measures of consideration are skin friction and local Nusselt number, which are defined and conveyed as follows:

$$C_f = \frac{2\tau_w}{\rho_f {U_w}^2}, \;\; Nu_x = \frac{xq_w}{k_f(T_w - T_\infty)}. \tag{11}$$

The Eq. 11 become non dimensional and defined as:

$$\begin{aligned} C_f Re^{\frac{1}{2}} &= \frac{\rho_F}{\rho_{hNF}}\left(\frac{\mu_{hNF}}{\mu_F}(1 - M\Theta(0)) + \frac{1}{\gamma_1} + \chi - n\chi\right)\left(H_{\xi\xi}(0)\right), \\ Nu_x Re^{-1/2} &= \frac{1}{Pr}\frac{(\rho c_p)_F}{(\rho c_p)_{hNF}}\left(\frac{k_{hNF}}{k_F}(1 + E\Theta(0)) + \frac{4}{3}Rd\right)\Theta_\xi(0). \end{aligned} \tag{12}$$

The Reynold number is Re.

3 Numerical procedure

The bvp4c numerical technique is used to solve nonlinear higher-order differential equations that have specific boundary conditions. This method involves breaking down the intricate higher-order differential system into a system of first-order differential equations, which can then be solved numerically. The model's convergence is achieved by reducing the residual error and achieving the tolerance threshold. The steps involved in this numerical technique include the following:

$$\begin{aligned} &X(1) = H(\xi);\, X(2) = H_\xi(\xi);\, H_{\xi\xi}(\xi) = X(3); H_{\xi\xi\xi}(\xi) = XX1;\, X(4) = G(\xi); \\ &X(5) = G_\xi(\xi);\;\; G_{\xi\xi\xi}(\xi) = XX2;\, \Theta(\xi) = X(6); X(7) = \Theta_\xi(\xi);\, \Theta_{\xi\xi}(\xi) = XX3; \end{aligned} \tag{13}$$

$$XX1 = \frac{-1}{\frac{\rho_F}{\rho_{hNF}}\frac{\mu_{hNF}}{\mu_F}\left(1+\frac{1}{\gamma_1}+\chi\right)(1+2\xi\mathrm{A})(1-MX(6))}($$
$$\left(2\frac{\rho_F}{\rho_{hNF}}\frac{\mu_{hNF}}{\mu_F}\left(1+\frac{1}{\gamma_1}+\chi\right)A(1-MX(6))X(3)-M(1+2\xi\mathrm{A})X(3)X(7)\right)+X(\quad (14)$$
$$-X(2)X(2)-\lambda\frac{\rho_F}{\rho_{hNF}}\frac{\mu_{hNF}}{\mu_F}(1-MX(6))X(2)-\Delta\frac{\rho_F}{\rho_{hNF}}X(2)\sin^2(\Pi)+\chi\frac{\rho_F}{\rho_{hN}}$$
$$+2\xi\mathrm{A})X(5)+2AX(4)));$$

$$XX2 = \frac{-1}{\frac{\rho_F}{\rho_{hNF}}\left(\frac{\mu_{hNF}}{\mu_F}+\frac{\chi}{2}\right)(1+2\xi\mathrm{A})(1-MX(6))}\left(\frac{\rho_F}{\rho_{hNF}}\left(\frac{\mu_{hNF}}{\mu_F}+\frac{\chi}{2}\right)\right.$$
$$(4A(1-MX(6))X(5)-M(1+2\xi\mathrm{A})X(7)X(5))+X(5)X(1)-AX(1)X(4)-2 \quad (15)$$
$$(4)-\frac{\chi}{2}\frac{\rho_F}{\rho_{hNF}}(X(4)+X(3))\Big);$$

$$XX3 = \frac{-1}{\frac{1}{Pr}\frac{(\rho c_p)_F}{(\rho c_p)_{hNF}}\left(\frac{k_{hNF}}{k_F}+\frac{4}{3}Rd\right)(1+2\xi\mathrm{A})(1+EX(6))}\left(\frac{1}{Pr}\frac{(\rho c_p)_F}{(\rho c_p)_{hNF}}\frac{k_{hNF}}{k_F}\right.$$
$$(2A(1+EX(6))X(7)+E(1+2\xi\mathrm{A})X(7)X(7))+\frac{4}{3}Rd(2AX(7))+X(7)X(1)- \quad (16)$$
$$)X(2)+S\frac{(\rho c_p)_F}{(\rho c_p)_{hNF}}X(6)\Big);$$

The boundary condition at surface:

$$X0(1)-Q;\ X0(2)-1;\ \ X\infty(2);\ \ X0(4)=-nX0(3);X\infty(4);X0(6)-1;\ \ X\infty(6); \quad (17)$$

4 Results and discussions

The system of differential equation which have developed under the flow assumptions and boundary layer approximations. The mathematical model have been cracked through numerical scheme and involving physical factor impact phenomena offered in the form of graphs and tabular form. Figs. 2-5 reported the physical features of external forces on velocity function. The velocity curves turn into increased due to addition in micropolar fluid factor which seen in Fig. 2. Micropolar factor has additional viscosity impacts due to the fluid microstructure. Higher values of the micropolar fluid parameter indicate a stronger interaction between the microelement and the fluid motion. Due to current phenomena, the velocity function increased. The impression of velocity and porosity factor presented in Fig. 3. The velocity curved reported to declining behaviour due to higher values of porosity factor. The current analysis of observed phenomena indicates that the relationship between a stretchable surface and fluid is inversely proportional according to Darcy's law. The fluid motion declined due to an augmentation in the porosity factor, which is resistance to declining fluid velocity.

The relation between nano concentration factor and velocity function which presented in Fig. 4. The velocity is noted to be decay due to upper values of nano concentration factor. With the rise in nanoparticle concentration, the effective viscosity of the fluid escalates. The communication between the nanoparticles and the fluid molecules, as well as among the nanoparticles themselves, creates additional internal friction, which in turn changes the behavior of the fluid. The higher viscosity means that the fluid encounters more resistance to flow, resulting in a reduction in the velocity profile. Fig. 5 reported the inversely relationship between fluid velocity and Casson fluid factor. The increment of the Casson fluid factor boosts the fluid viscosity. Due to the increment in viscosity, the viscosity resists fluid motion and velocity decline near the surface. Fig. 6 presented the influence of micropolar rotation factor on micro rotation profile. Curved of micro rotation profile boosted up due to increment in micro rotation profile. The thicker boundary layer impact developed due to an increment in the micropolar factor as well as micropolar rotational profile increased. This leads to an upsurge in the microrotation profile as the microelements participate more actively in the flow dynamics. Fig. 7 reported the effects of nanoconcentration on micropolar profile. The curved of micropolar profile is noted to be decline by higher values of nanoparticle concentration factor. With higher nanoparticle concentration, the boundary layer may become thinner, affecting the distribution of microrotation near the stretching surface. A thinner boundary layer means less space for microrotation effects to manifest, leading to a decline in the micropolar profile. Figs. 8-11 revealed the inspiration of physical factor on the temperature. Fig. 8 emphasised the impressions of variable thermal conductivity on temperature. The temperature become higher by increasing values of variable thermal conductivity. Thermal conductivity and temperature of fluid directly relation. The thermal conductivity boosted up ultimately, temperature of fluid boosted up. The deviation of temperature and nanoparticle concentration revealed in Fig. 9. The temperature noted to be higher due to increment in nanoparticle concentration. Nanoparticles can also alter the convective heat transfer characteristics of the fluid. As nano concentration upsurges, the convective heat transfer coefficient can change, affecting heat transport within the fluid. Changes in heat transfer dynamics lead to higher temperatures in regions influenced by nanoparticles. Fig. 10 is offered the inspiration of thermal radiation on temperature. The temperature revealed to be enhance due to enlarging values of radiation. The deviation of temperature and heat generation revealed in Fig. 11. Temperature noted to be higher due to increment in heat generation. The additional heat energy diffuses and rises the temperature of the surrounding fluid.

Table 2 reported the effect of casson factor, micropolar factor, variable viscosity, heat generation, radiation, porosity factor, variable thermal conductivity, suction factor, magnetic field and nanoconcentration on the Nusselt number and skin friction. The magnitude of skin friction increased while Nusselt number reduced by enlarging values of casson fluid factor. The magnitude of skin friction declined and Nusselt number increased by enlarging values of micropolar factor. As the micropolar factor rises, the micro-rotational effects within the fluid change the velocity and stress distributions near the surface. This change often decreases the velocity gradient at the boundary, reducing skin friction. The increased micropolar effects improve the fluid's ability to carry heat away from the surface, leading to higher heat transfer rates and, consequently, higher Nusselt numbers. Nusselt number declined while magnitude of skin friction boosted up by higher values of variable viscosity factor. An increase in viscosity means increased resistance to flow near the surface. Consequently, the velocity gradient at the surface increases, leading to higher shear stress and, consequently, higher skin friction. This decrease occurs because higher viscosity tends to reduce the fluid's ability to carry heat away from the surface efficiently. The slower-moving fluid near the surface reduces convective heat transfer rates, resulting in a lower Nusselt number. Nusselt number and magnitude of skin friction declined due to higher values of heat generation. Higher heat generation can change the velocity and temperature near the surface. It can lead to reduced velocity gradients at the surface due to buoyancy effects, especially in buoyancy-assisted flows. The reduction in velocity gradients tends to decrease the skin friction coefficient. Higher heat generation can lead to a decrease in skin friction. Rise in the temperature gradient tends to enhance the convective heat transfer from the surface to the fluid. Nusselt number tends to increase with higher heat generation rates. Nusselt number and magnitude of skin friction declined due to upper values of radiation. The Nusselt number declined due to radiation being more significant than convection. The phenomena exist due to radiation changing the temperature at the surface because the thermal boundary layer is directly affected and potentially lowers the convective heat transfer coefficient. Due to that reason, fluid viscosity near the wall declined, which reduced skin friction. Nusselt number reduced while magnitude of skin friction increased by enlarging values of porosity factor. The higher porosity of the surface allows fluid more to pass through it because it changes the flow dynamic which increased the shear stress and skin friction. The higher porosity of the surface allows fluid more to pass through it which reduced the surface temperature. Magnitude of skin friction and Nusselt number decayed due to higher values of variable thermal conductivity. Magnitude of skin friction and Nusselt number deteriorated due to

higher values of suction factor. Magnitude of skin friction increased while Nusselt number reduced by enlarging values of magnetic field. The magnitude of skin friction increased while Nusselt number reduced by enlarging values of nano concentration. The presence of nanoparticles in the fluid can change its flow characteristics, potentially leading to an increase in viscosity. This change usually results in higher shear stress at the surface, causing an rise in skin friction. Additionally, the nanoparticles may impede convective heat transfer by affecting flow patterns or reducing heat transfer coefficients, ultimately producing a reduction in the Nusselt number. Table 3 presented the comparison our work with Nadeem et al. [40] for diverse values of Pr when rest of the values consider zero. Fig. 12 reported the comparative results of stretching sheet / cylinder for both hybrid casson micropolar nanofluid and casson micropolar nanofluid. The heat transfer of sheet achieved more as compared to stretching cylinder. In this model, the cooling effects are point into current analysis.

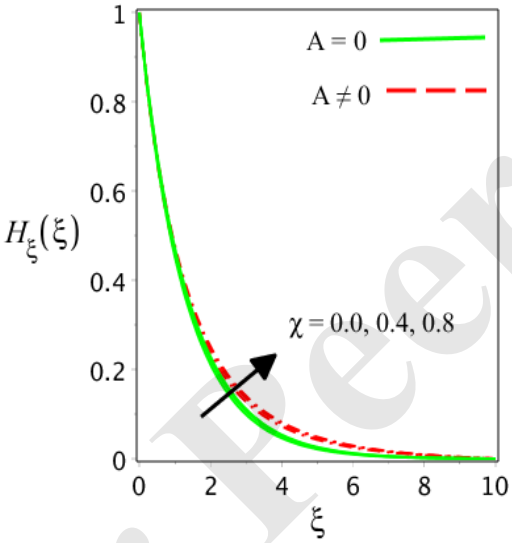

Fig. 2: Variation of χ and velocity.

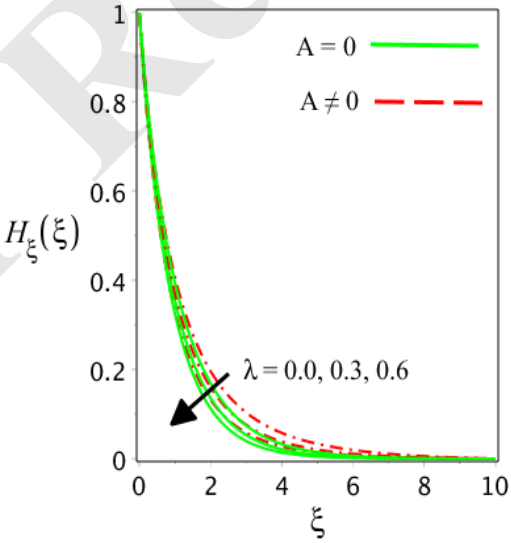

Fig. 3: Variation of λ and velocity.

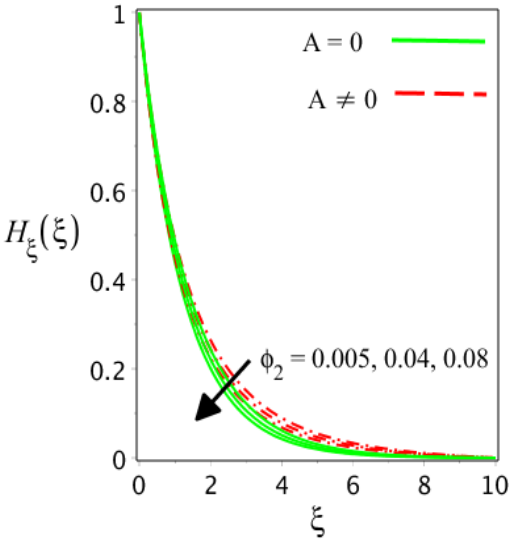

Fig. 4: Variation of ϕ_2 and velocity.

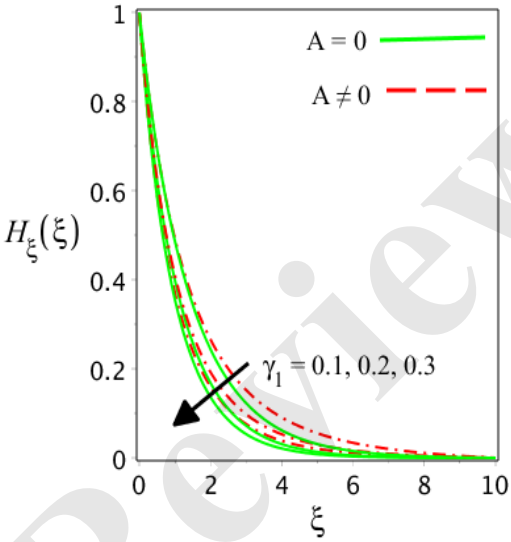

Fig. 5: Variation of $\gamma_1$and velocity.

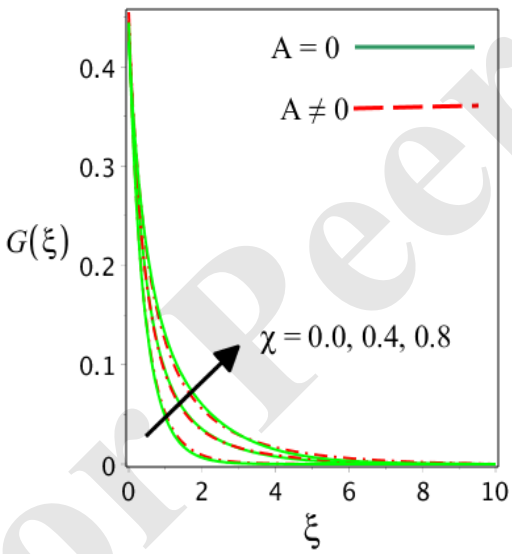

Fig. 6: Variation of χ and micropolar.

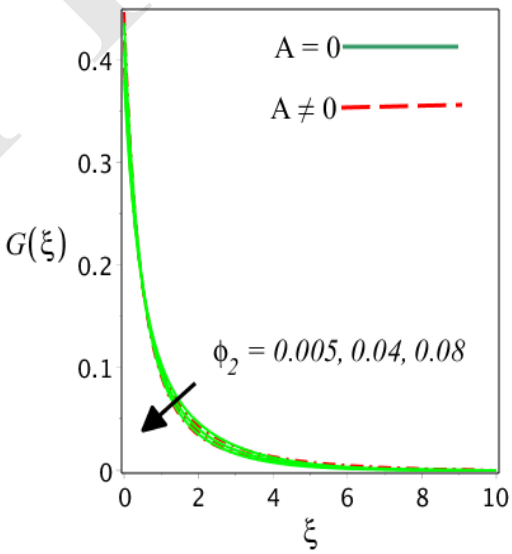

Fig. 7: Variation of ϕ_2 and micropolar.

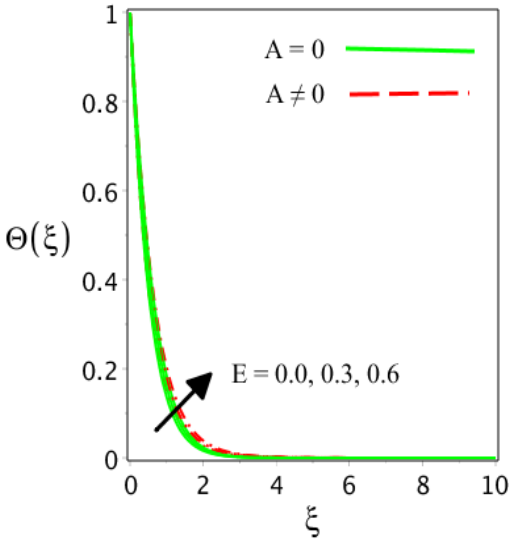

Fig. 8: Variation of E and temperature.

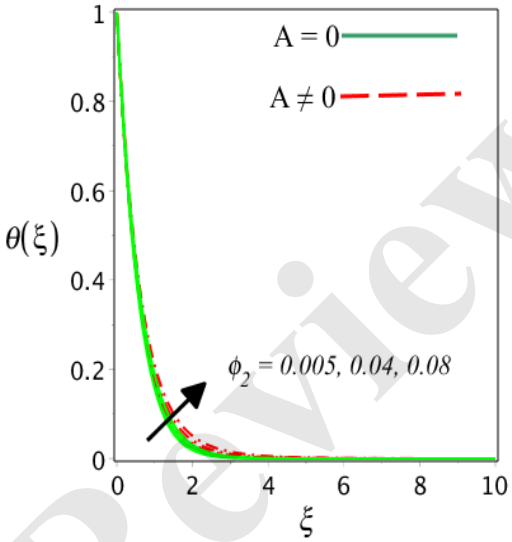

Fig. 9: Variation of ϕ_2 and temperature.

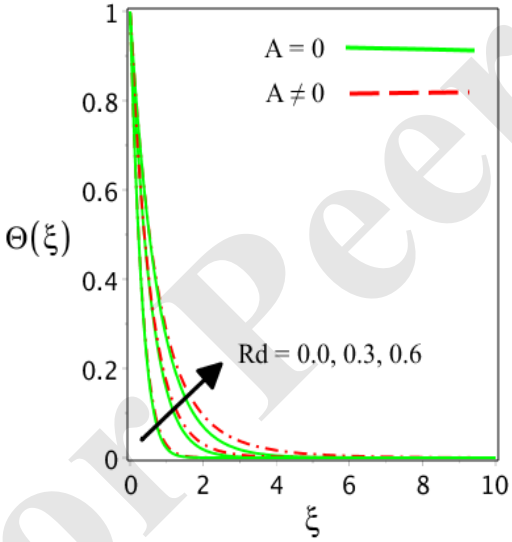

Fig. 10: Variation of Rd and temperature.

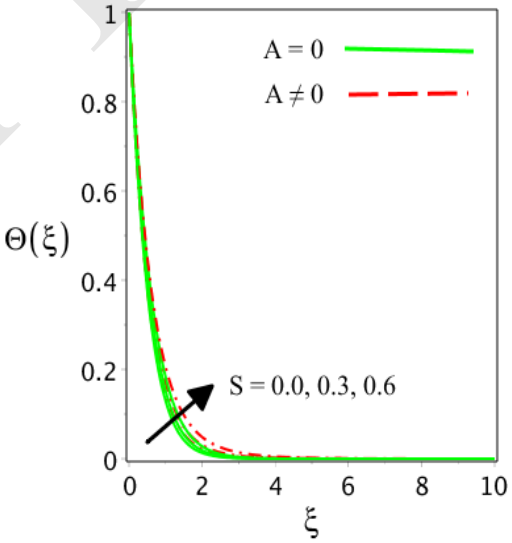

Fig. 11: Variation of S and temperature.

Table 2: Numerical outcome of $-C_f Re^{\frac{1}{2}}$ and $Nu_x Re^{-1/2}$ for different values of physical factors.

Physical factors										Stretching Cylinder		Stretching Sheet	
γ_1	χ	M	S	Rd	λ	E	Q	Δ	ϕ_2	$Nu_x Re^{-1/2}$	$-C_f Re^{\frac{1}{2}}$	$Nu_x Re^{-1/2}$	$-C_f Re^{\frac{1}{2}}$
0.1	0.4	0.4	0.3	0.3	0.4	0.4	0.3	0.2	0.04	2.92037840	2.22443261	2.86832237	2.09492585
0.2	-	-	-	-	-	-	-	-	-	2.84152400	3.00371071	2.78901735	2.89487914
0.3	-	-	-	-	-	-	-	-	-	2.78536014	4.60836833	2.73328022	4.48102312

0.4	-	-	-	-	-	-	-	-	-	2.69563201	4.87954212	2.63319672	4.69704576
0.3	0.0	-	-	-	-	-	-	-	-	2.77554982	4.70303533	2.72369477	4.57551288
-	0.4	-	-	-	-	-	-	-	-	2.78536014	4.60836833	2.73328022	4.48102312
-	0.8	-	-	-	-	-	-	-	-	2.79440622	4.49516944	2.74190719	4.37001656
-	1.2	-	-	-	-	-	-	-	-	2.80299019	4.37372834	2.74994488	4.25214585
-	0.4	0.1	-	-	-	-	-	-	-	2.79444422	4.09416419	2.74592031	3.91050710
-	-	0.2	-	-	-	-	-	-	-	2.79154448	4.14738533	2.74186204	3.98506592
-	-	0.3	-	-	-	-	-	-	-	2.78851802	4.20433213	2.73765077	4.06392736
-	-	0.4	-	-	-	-	-	-	-	2.78536014	4.26538833	2.73328022	4.14752091
-	-	0.4	0.1	-	-	-	-	-	-	2.93343707	4.27412032	2.87760326	4.15268786
-	-	-	0.2	-	-	-	-	-	-	2.86099382	4.26994065	2.80682023	4.15019852
-	-	-	0.3	-	-	-	-	-	-	2.78536014	4.26538833	2.73328022	4.14752090
-	-	-	0.4	-	-	-	-	-	-	2.70586890	4.26036224	2.65656377	4.14461991
-	-	-	0.3	0.0	-	-	-	-	-	4.40716214	4.34870277	4.35972972	4.19975963
-	-	-	-	0.3	-	-	-	-	-	2.78536014	4.26538833	2.73328022	4.14752091
-	-	-	-	0.6	-	-	-	-	-	2.13063582	4.21583595	2.07964405	4.11668299
-	-	-	-	0.9	-	-	-	-	-	1.75310869	4.18042195	1.70292333	4.09452007
-	-	-	-	0.3	0.0	-	-	-	-	2.82459906	3.87176830	2.77043810	3.75635289
-	-	-	-	-	0.4	-	-	-	-	2.78536013	4.26538833	2.73328022	4.14752091
-	-	-	-	-	0.8	-	-	-	-	2.74990145	4.60840256	2.69987184	4.49015430
-	-	-	-	-	1.2	-	-	-	-	2.71706547	4.91500111	2.66916108	4.79772569
-	-	-	-	-	0.4	0.0	-	-	-	3.09841913	4.27678468	3.04322274	4.15470977
-	-	-	-	-	-	0.2	-	-	-	2.93152828	4.27096777	2.87800362	4.15103985
-	-	-	-	-	-	0.4	-	-	-	2.78536014	4.26538833	2.73328022	4.14752091
-	-	-	-	-	-	0.6	-	-	-	2.65613121	4.26002865	2.60531236	4.14414166
-	-	-	-	-	-	0.4	0.0	-	-	2.42611184	3.93843908	2.37093567	3.81704215
-	-	-	-	-	-	-	0.3	-	-	2.78536014	4.26538833	2.73328022	4.14752091
-	-	-	-	-	-	-	0.6	-	-	3.18486243	4.61251929	3.13683268	4.50001085
-	-	-	-	-	-	-	0.9	-	-	3.62004268	4.97897823	3.57645093	4.87349805
-	-	-	-	-	-	-	0.3	0.0	-	2.79773894	4.13306606	2.74502053	4.01557173
-	-	-	-	-	-	-	-	0.2	-	2.78536014	4.26538833	2.73328022	4.14752091
-	-	-	-	-	-	-	-	0.4	-	2.77329766	4.39299941	2.72185719	4.27494828
-	-	-	-	-	-	-	-	0.6	-	2.76151804	4.51633467	2.71072125	4.39826608
-	-	-	-	-	-	-	-	0.2	0.005	2.97341465	4.06202743	2.91921598	3.93450913
-	-	-	-	-	-	-	-	-	0.02	2.93638983	4.18056662	2.88225508	4.05652921
-	-	-	-	-	-	-	-	-	0.04	2.88830058	4.33217137	2.83429591	4.21245849
-	-	-	-	-	-	-	-	-	0.06	2.84160322	4.47678328	2.78778083	4.36106912

Table 3: Comparison present work with Nadeem et al. [40] for different values of Pr when rest of the values consider zero.

Pr	Nadeem et al. [10]	Present analysis
1.00	0.95470	0.954680
2.00	1.47140	1.471380
3.00	1.89610	1.895760

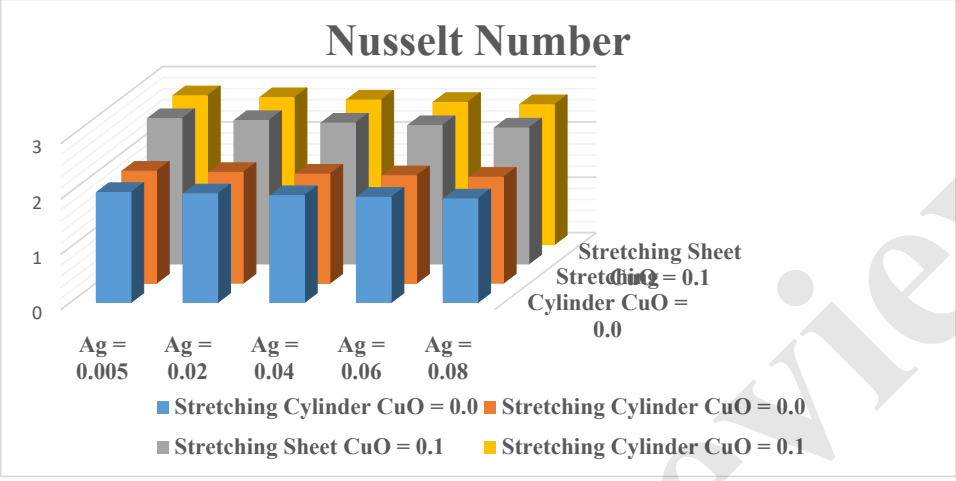

Fig. 12: Comparative results of stretching sheet / cylinder for both hybrid casson micropolar nanofluid and casson micropolar nanofluid.

5 Final remarks

We analyzed a Casson micropolar hybrid nanofluid flow and heat transfer characteristics over a stretching sheet/cylinder. The analysis takes into account Joule heating and thermal radiation, as well as variable thermal conductivity and viscosity. Additionally, the study explores the influence of an inclined magnetic field on the flow behavior. The governing partial differential equations, representing the conservation of mass, momentum, and energy, are reformulated into a nonlinear ordinary differential equation through suitable similarity transformations. These transformed equations are then solved numerically using a robust computational method. The main key point results have been highlighted below:

- The velocity curved reported to declining behaviour due to sophisticating values of porosity factor. The fluid motion declined due to an increment in the porosity factor, which is resistance to declining fluid velocity.
- The temperature become higher by expanding values of variable thermal conductivity. Thermal conductivity and temperature of fluid have directly relation. Thermal conductivity boosted up ultimately, fluid temperature enhanced.
- The temperature noted to be higher due to increment in heat generation. The additional heat energy diffuses and increases the fluid temperature.

- The heat transfer of sheet achieved more as compared to stretching cylinder. In this model, the cooling effects are point into current analysis.

Availability of data and material: Not Applicable

Competing interests: All the authors have no Conflict of interests.

References

1. Eringen, A. C. (1969). Micropolar fluids with stretch. *International Journal of Engineering Science*, *7*(1), 115-127.
2. Kazakia, Y., & Ariman, T. (1971). Heat-conducting micropolar fluids. *Rheologica Acta*, *10*(3), 319-325.
3. Char, M. I., & Chang, C. L. (1997). Effect of wall conduction on natural convection flow of micropolar fluids along a flat plate. *International journal of heat and mass transfer*, *40*(15), 3641-3652.
4. Tomar, S. K., & Kumar, R. (1999). Elastic wave propagation in a cylindrical bore situated in a micropolar elastic medium with stretch. *Proceedings-Mathematical Sciences*, *109*, 425-433.
5. Elbarbary, E. M. E., & Elgazery, N. S. (2005). Flow and heat transfer of a micropolar fluid in an axisymmetric stagnation flow on a cylinder with variable properties and suction (numerical study). *Acta Mechanica*, *176*, 213-229.
6. Rehman, A., Bazai, R., Achakzai, S., Iqbal, S., & Naseer, M. (2015). Boundary layer flow and heat transfer of micropolar fluid over a vertical exponentially stretched cylinder. *App Comp Math*, *4*(6), 424-430.
7. Abbas, N., Saleem, S., Nadeem, S., Alderremy, A. A., & Khan, A. U. (2018). On stagnation point flow of a micro polar nanofluid past a circular cylinder with velocity and thermal slip. *Results in Physics*, *9*, 1224-1232.
8. Khan, A. A., Abbas, N., Nadeem, S., Shi, Q. H., Malik, M. Y., Ashraf, M., & Hussain, S. (2021). Non-Newtonian based micropolar fluid flow over nonlinear starching cylinder under Soret and Dufour numbers effects. *International Communications in Heat and Mass Transfer*, *127*, 105571.
9. Nawaz, Y., Arif, M. S., & Abodayeh, K. (2023). Unconditionally stable numerical scheme for heat transfer of mixed convective darcy–forchheimer flow of micropolar fluid over oscillatory moving sheet. *Journal of Computational and Nonlinear Dynamics*, *18*(4), 041006.
10. Abbas, N., Shatanawi, W., & Shatnawi, T. A. (2024). Thermodynamic properties of Casson-Sutterby-micropolar fluid flow over exponential stretching curved sheet with impact of MHD and heat generation. *Case Studies in Thermal Engineering*, *55*, 104123.
11. Choi, S. U., & Eastman, J. A. (1995). *Enhancing thermal conductivity of fluids with nanoparticles* (No. ANL/MSD/CP-84938; CONF-951135-29). Argonne National Lab.(ANL), Argonne, IL (United States).

12. Li, J., & Kleinstreuer, C. (2008). Thermal performance of nanofluid flow in microchannels. *International Journal of Heat and Fluid Flow*, *29*(4), 1221-1232.
13. Gorla, R. S. R., El-Kabeir, S. M. M., & Rashad, A. M. (2011). Boundary-layer heat transfer from a stretching circular cylinder in a nanofluid. *Journal of thermophysics and heat transfer*, *25*(1), 183-186.
14. Suresh, S., Venkitaraj, K. P., Selvakumar, P., & Chandrasekar, M. (2011). Synthesis of Al2O3–Cu/water hybrid nanofluids using two step method and its thermo physical properties. *Colloids and Surfaces A: Physicochemical and Engineering Aspects*, *388*(1-3), 41-48.
15. Sarkar, J., Ghosh, P., & Adil, A. (2015). A review on hybrid nanofluids: recent research, development and applications. *Renewable and Sustainable Energy Reviews*, *43*, 164-177.
16. Huminic, G., & Huminic, A. (2020). Entropy generation of nanofluid and hybrid nanofluid flow in thermal systems: a review. *Journal of Molecular Liquids*, *302*, 112533.
17. Alghamdi, W., Alsubie, A., Kumam, P., Saeed, A., & Gul, T. (2021). MHD hybrid nanofluid flow comprising the medication through a blood artery. *Scientific Reports*, *11*(1), 11621.
18. Alsaedi, A., Muhammad, K., & Hayat, T. (2022). Numerical study of MHD hybrid nanofluid flow between two coaxial cylinders. *Alexandria Engineering Journal*, *61*(11), 8355-8362.
19. Li, S., Saadeh, R., Madhukesh, J. K., Khan, U., Ramesh, G. K., Zaib, A., ... & Sherif, E. S. M. (2024). Aspects of an induced magnetic field utilization for heat and mass transfer ferromagnetic hybrid nanofluid flow driven by pollutant concentration. *Case Studies in Thermal Engineering*, *53*, 103892.
20. Mebarek-Oudina, F., Chabani, I., Vaidya, H., & Ismail, A. A. I. (2024). Hybrid-nanofluid magneto-convective flow and porous media contribution to entropy generation. *International Journal of Numerical Methods for Heat & Fluid Flow*, *34*(2), 809-836.
21. Batra, R. L., & Das, B. (1992). Flow of a Casson fluid between two rotating cylinders. *Fluid dynamics research*, *9*(1-3), 133.
22. Pandey, S. K., & Tripathi, D. (2010). Peristaltic transport of a Casson fluid in a finite channel: application to flows of concentrated fluids in oesophagus. *International Journal of Biomathematics*, *3*(04), 453-472.
23. Malik, M. Y., Naseer, M., Nadeem, S., & Rehman, A. (2014). The boundary layer flow of Casson nanofluid over a vertical exponentially stretching cylinder. *Applied Nanoscience*, *4*, 869-873.
24. Tulu, A., & Ibrahim, W. (2020). Spectral relaxation method analysis of Casson nanofluid flow over stretching cylinder with variable thermal conductivity and Cattaneo–Christov heat flux model. *Heat Transfer*, *49*(6), 3433-3455.
25. Nawaz, Y., Arif, M. S., & Abodayeh, K. (2023). Predictor–corrector scheme for electrical magnetohydrodynamic (MHD) Casson nanofluid flow: a computational study. *Applied Sciences*, *13*(2), 1209.
26. Arif, M. S., Abodayeh, K., & Nawaz, Y. (2023). Design of finite difference method and neural network approach for casson nanofluid flow: a computational study. *Axioms*, *12*(6), 527.

27. Mahabaleshwar, U. S., Maranna, T., Mishra, M., Hatami, M., & Sunden, B. (2024). Radiation effect on stagnation point flow of Casson nanofluid past a stretching plate/cylinder. *Scientific Reports*, *14*(1), 1387.
28. Nasir, M., Kausar, M. S., Waqas, M., Beg, O. A., & Khan, W. A. (2024). Computational analysis of magnetized Casson liquid stretching flow adjacent to a porous medium with Joule heating, stratification, multiple slip and chemical reaction aspects. *Numerical Heat Transfer, Part A: Applications*, 1-23.
29. Ali, M. Y., Reza-E-Rabbi, S., Ahmmed, S. F., Nabi, M. N., Azad, A. K., & Muyeen, S. M. (2024). Hydromagnetic flow of Casson nano-fluid across a stretched sheet in the presence of thermoelectric and radiation. *International Journal of Thermofluids*, *21*, 100484.
30. Wang, C. Y. (1988). Fluid flow due to a stretching cylinder. *Physics of Fluids*, *31*(3), 466-468.
31. Ishak, A., Nazar, R., & Pop, I. (2008). Uniform suction/blowing effect on flow and heat transfer due to a stretching cylinder. *Applied Mathematical Modelling*, *32*(10), 2059-2066.
32. Mastroberardino, A., & Paullet, J. E. (2010). Existence and a priori bounds for steady stagnation flow toward a stretching cylinder. *Journal of mathematical analysis and applications*, *365*(2), 701-710.
33. Malik, M. Y., Hussain, A., Salahuddin, T., & Awais, M. (2016). Numerical solution of MHD Sisko fluid over a stretching cylinder and heat transfer analysis. *International Journal of Numerical Methods for Heat & Fluid Flow*, *26*(6), 1787-1801.
34. Usman, M., Soomro, F. A., Haq, R. U., Wang, W., & Defterli, O. (2018). Thermal and velocity slip effects on Casson nanofluid flow over an inclined permeable stretching cylinder via collocation method. *International Journal of Heat and Mass Transfer*, *122*, 1255-1263.
35. Bilal, M., Saeed, A., Selim, M. M., Gul, T., Ali, I., & Kumam, P. (2021). Comparative numerical analysis of Maxwell's time-dependent thermo-diffusive flow through a stretching cylinder. *Case Studies in Thermal Engineering*, *27*, 101301.
36. Mohanty, D., Mahanta, G., & Shaw, S. (2024). Irreversibility and thermal performance of nonlinear radiative cross-ternary hybrid nanofluid flow about a stretching cylinder with industrial applications. *Powder Technology*, *433*, 119255.
37. Alghamdi, M., Akbar, N. S., Zamir, T., & Muhammad, T. (2024). Double layered combined convective heated flow of Eyring-Powell fluid across an elevated stretched cylinder using intelligent computing approach. *Case Studies in Thermal Engineering*, *54*, 104009.
38. Qadan, H., Alkasasbeh, H., Yaseen, N., Sawalmeh, M. Z., & ALKhalafat, S. (2019). A Theoretical study of steady MHD mixed convection heat transfer flow for a horizontal circular cylinder embedded in a micropolar casson fluid with thermal radiation. *Journal of Computational Applied Mechanics*, *50*(1), 165-173.
39. Abbas, N., Shatanawi, W., Hasan, F., & Shatnawi, T. A. (2025). Investigation of MHD radiative casson micropolar hybrid nanofluid over exponential curved stretching sheet. *Journal of Radiation Research and Applied Sciences*, *18*(1), 101269.

40. Nadeem, S., Ullah, N., Khan, A. U., & Akbar, T. (2017). Effect of homogeneous-heterogeneous reactions on ferrofluid in the presence of magnetic dipole along a stretching cylinder. *Results in physics*, *7*, 3574-3582.